Hybrid Pulse Position Modulation/Ultrashort Light Pulse Code-Division Multiple-Access Systems—Part II: Time–Space Processor and Modified Schemes

Kwang Soon Kim, *Member, IEEE*, Dan M. Marom, *Member, IEEE*, Laurence B. Milstein, *Fellow, IEEE*, and Yeshaiahu Fainman, *Fellow, IEEE*

Abstract—In Part I of this two-part paper, we proposed and investigated a hybrid pulse position modulation/ultrashort light pulse code-division multiple-access (PPM/ULP-CDMA) system for ultrafast optical communication networks. In the proposed scheme, the large bandwidth of an ULP is efficiently utilized by virtue of the very high time resolution of a time–space processor. In this paper, more detailed analysis and discussion on the receiver scheme using the time–space processor is presented; nonideal performance of the time–space processor, including the reference pulse realization problem, as well as amplifier and detector noise, are taken into account. Discussions on physically achievable ranges of the system parameters that determine the performance of the proposed PPM/ULP-CDMA system are also made based upon current, state of the art technology. As remedies to overcome the physical limitations on the system parameters, two modified modulation/demodulation schemes are proposed and investigated to enhance the performance of the hybrid PPM/ULP-CDMA system.

Index Terms—Optical code-division multiple access (CDMA), pulse position modulation (PPM), time–space processor, ultrashort light pulse (ULP).

I. INTRODUCTION

IN [1], we proposed and investigated a hybrid pulse position modulation/ultrashort light pulse code-division multiple-access (PPM/ULP-CDMA) system to provide ultrafast communication in multiple-access optical networks. In the proposed hybrid PPM/ULP-CDMA system, a pulse position modulation (PPM) format with very short pulse separation was used to utilize the given large bandwidth of an ultrashort
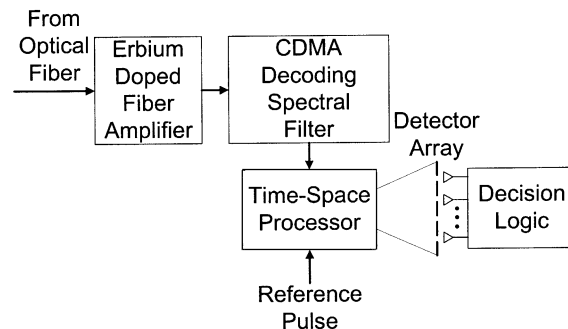
Fig. 1. Receiver scheme of the hybrid PPM/ULP-CDMA system.

light pulse (ULP) efficiently. In order to successfully detect the ultrafast signal, we proposed a time–space processor with a photodetector array as a receiver scheme. The performance of the hybrid PPM/ULP-CDMA system was analyzed by assuming the time–space processor was ideal and the interuser interference was the dominant source of performance degradation, as usually assumed in optical CDMA systems. However, to perform a solid investigation on the hybrid PPM/ULP-CDMA system, effects such as the nonideal amplitude characteristic of the time–space processor, methods for obtaining the reference pulse for synchronization, amplifier and detector noise, and the nonideal characteristics of fiber transmission, including dispersion and nonlinear distortion, should be taken into account.

In this paper, we study such nonideal effects on the performance of the hybrid PPM/ULP-CDMA system. In Sections II–IV, the receiver of the proposed PPM/ULP-CDMA system using a time–space processor, shown in Fig. 1, is discussed in detail. An incoming temporal signal is first amplified by an erbium doped fiber amplifier (EDFA) and transformed linearly into a spatial signal by the time–space processor. The spatial signal is then detected by a photodetector array and decision logic. In Section II, the time-to-space conversion process is briefly introduced. The time–space processor considered in this paper was originally proposed in [2] to perform femtosecond pulse imaging using a nonlinear three-wave mixing process. In [3], more detailed analysis was performed with a focus on the time-to-space conversion characteristic of the ultrafast signal, and showed that the time–space processor converted the incoming temporal signal into an output spatial image linearly with nonuniform energy conversion efficiency when the processor operated in the linear-conversion regime. The energy
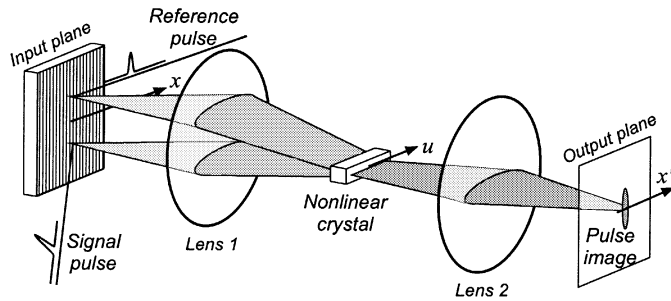
Fig. 2.   Schematic of the time–space processor.

conversion efficiency was also formulated and, with reasonable parameters, was typically low (0.1%–1%).[1] To compensate for the low energy conversion efficiency of the time–space processor, an optical amplifier is implemented. In Section III, amplifier and detector noise, as well as some nonideal effects of the time–space processor on the performance of the proposed system, are investigated in terms of input and output signal-to-noise ratios (SNR) of a photodetector. In Section IV, some design issues on the hybrid PPM/ULP-CDMA system are considered. In addition, realization of a reference pulse, which is required for the time-to-space conversion process in the time–space processor, is discussed. In Section V, two modified schemes to enhance the performance of the proposed PPM/ULP-CDMA system are investigated.

II. ULTRAFAST DETECTION WITH THE TIME–SPACE PROCESSOR

Detecting the information-carrying ULPs of the PPM/ULP-CDMA format requires all-optical processing, as the processing is occurring at a rate that exceeds the capabilities of electronics. Since the detection is required to operate in real time and over a large time window, we utilize a new ultrafast waveform imaging technique that efficiently converts the temporal information to a spatial distribution [2]. The spatial information can be detected by an array of slower detectors. The ultrafast waveform imaging technique is based on a nonlinear three-wave mixing process in a spectral processing device (SPD) (see Fig. 2). The two input waves are derived from the received signal of the optical network and from a reference pulse that is either locally generated or provided by the network. The wave-mixing process produces a quasi-monochromatic output wave, carrying the information of the signal waveform. The optical signal at the output plane of the SPD is proportional to the complex amplitude of the ultrafast waveform. The detection process occurs after the CDMA despreading filter has recompressed the desired user's pulse back to an ULP, while the other users' signals remain spread. At this point, we assume that the fiber transmission does not introduce any distortion to the transmitted signals. Let $s(t)$ and $r_{\text{ref}}(t)$ be the baseband equivalent waveforms at the output of the CDMA despreading filter and the reference pulse used as input to the time–space processor, respectively. Then, they may be

specified as $s(t) = \sqrt{P_0}p_\tau(t - (X - X_c)T_{\text{ps}}) + \sqrt{P_0}v(t)$ and $r_{\text{ref}}(t) = \sqrt{P_{ref}}p_\tau(t)$, respectively, where $p_\tau(t) = p_u(t/\tau)$ is an arbitrary baseband ULP shape with duration τ, and where the properties of $p_u(t)$ were defined in [1], P_0 and P_{ref} are the peak powers of the received and reference ULP's, respectively, $v(t)$ is the baseband equivalent CDMA despreading filter output due to the interuser interference, normalized by $\sqrt{P_0}$, T_{ps} is the separation between the adjacent PPM symbols, X represents the data symbol of the desired user, and $X_c = (M - 1)/2$ represents time shift to adjust the center position of the PPM symbols. The two waveforms are incident on the diffraction gratings at the input plane of the SPD, giving rise to the input fields [3]

$$U_1(x;t) = w\left(\frac{x}{L}\right) s\left(t - \frac{\zeta x}{c}\right) \exp(j\omega_0 t) \qquad (1)$$

and

$$U_2(x;t) = w\left(\frac{x}{L}\right) r_{\text{ref}}\left(t + \frac{\zeta x}{c}\right) \exp(j\omega_0 t). \qquad (2)$$

Although the input fields are actually two-dimensional (2-D), we consider only the x direction, since the detection information resides in only the x direction. The pupil function, $w(\cdot)$, defines the spatial mode of the beam on the diffraction grating, where L is its width, ζ is a constant that depends on the grating spatial frequency, c is the speed of light, and $\omega_0 = 2\pi f_0$, where f_0 is the optical carrier frequency. Equations (1) and (2) describe a temporal signal propagating across the pupil at velocity c/ζ and $-c/\zeta$, respectively, due to the illumination of the input optical signals at opposite angles on the grating. The finite span of the temporal signal due to the spatial mode size serves as the time window of the device. The input fields are spatially Fourier transformed by a lens, and generate a new optical wave by the nonlinear mixing process that is proportional to the product of the two input waves in the spatial frequency domain [4]. The resultant signal is spatially Fourier transformed to the output plane of the processor, giving rise to the output field

$$U_{out}(x'';t) \propto \left(s\left(\frac{2\zeta x''}{c}\right) \otimes r_{\text{ref}}\left(-\frac{2\zeta x''}{c}\right) \right) w\left(-\frac{ct}{\zeta L}\right)$$
$$\cdot w\left(\frac{ct}{\zeta L} - \frac{2x''}{L}\right) \exp(j2\omega_0 t) \quad (3)$$

where $\otimes$ denotes the convolution operation. Note that the carrier frequency is doubled. Since 1550 nm-wavelength light is commonly used in fiber-optic communications, the resultant carrier wavelength is near 800 nm, which fortunately coincides with the peak absorption of silicon. Thus, cheap and well-developed silicon photodetectors can easily be used in the proposed scheme. In developing (3), we used the approximation that the instantaneous width of the reference pulse in (2) is much smaller than the input pupil functions to simplify the expression. The temporal information of $s(\cdot)$ and $r_{\text{ref}}(\cdot)$ appears as a stationary spatial signal, and its duration is determined by the pupil function $w(\cdot)$. However, in detecting the signal at the output plane, the sensing device registers the optical intensity and operates at a slow rate. Therefore, the detected

signal is given by

$$
S_{\text{out}}(x'') = \int\limits_{-\infty}^{\infty} |U_{\text{out}}(x'';t)|^2 \, dt
$$

$$
\propto \left| s\left(\frac{2\zeta x''}{c}\right) \otimes r_{\text{ref}}\left(-\frac{2\zeta x''}{c}\right) \right|^2
$$

$$
\cdot \int\limits_{-\infty}^{\infty} w^2\left(-\frac{2x''}{L} - \xi\right) w^2(\xi) d\xi. \tag{4}
$$

The convolution integral of the input pupil functions limits the range x'' of the output spatial signal. Subsequently, this limits the observed input temporal signal. Additional insight to the output detected signal is gained if we introduce a Gaussian model for the input beam profiles, i.e., $w(x) = \exp(-x^2)$. Using the Gaussian mode model, the integral in (4) can be evaluated, and inserting the definitions for the signal and reference waveforms yields

$$
S_{\text{out}}(x'') \propto \left| \left(p_\tau\left(\frac{2\zeta x''}{c} - (X - X_c)T_{\text{ps}}\right) + v\left(\frac{2\zeta x''}{c}\right) \right) \right.
$$
$$
\left. \otimes p_\tau\left(-\frac{2\zeta x''}{c}\right) \right|^2 \exp\left(-\frac{4x''^2}{L^2}\right). \tag{5}
$$

From (5), we see that a data pulse is detected at location $x'' = c(X - X_c)T_{\text{ps}}/2\zeta$, and is attenuated by $\exp(-4x''^2/L^2) = \exp(-(c(X - X_c)T_{\text{ps}}/\zeta L)^2)$ due to the processor's time window. It is apparent that the detected signal level from each possible pulse position is different. However, the attenuation is known *a priori* and affects the desired signal and interference in the same manner, and can, therefore, be taken into consideration in the decision logic (that is, normalizing by the attenuation) if detector noise is negligible. More detailed optical analysis of the time–space processor is available in [3].

III. AMPLIFIER AND DETECTOR NOISE

In Section II, the time–space processor was considered to convert fast temporal signals into spatial images to perform fast signal detection. The energy conversion efficiency of the time–space processor is formulated in [3], and, with reasonable parameters and reference pulse energy, the energy conversion efficiency is typically low (0.1%–1%). In addition, transmitted power must be sufficiently small to prevent nonlinear distortion during propagation in the fiber. Thus, a large-gain optical amplifier may be required to compensate for the energy conversion loss in the time–space processor. On the other hand, as will be shown later, a small photodetector size is desirable to maximize the signal-to-interuser interference ratio, which, in turn, reduces incident average power to a photodetector. In this case, detector noise may not be negligible. In this section, the effect of the amplifier and detector noise on the input and output SNR of a photodetector is investigated.

The receiver using the time–space processor and an equivalent receiver are illustrated in Figs. 1 and 3, respectively. The output from the fiber passes through an optical amplifier,
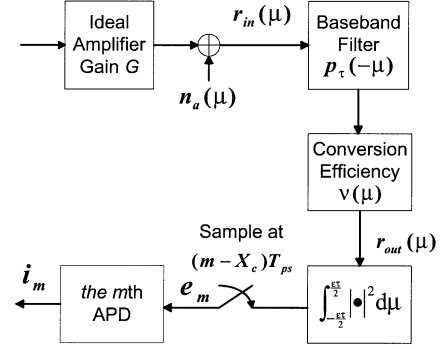

Fig. 3.   An equivalent receiver scheme.

a CDMA despreading filter, and the time–space processor. After passing through the time–space processor, a temporal signal, as a function of the time variable, t, is converted into a spatial signal, as a function of the spatial variable, $x'' = ct/2\zeta$. Then, the spatial signal is integrated and dumped over the physical size of a photodetector, D, in the spatial domain. On the other hand, temporal variation in the output of the time–space processor is determined by the pupil function, $w(\cdot)$, of the grating, and is integrated over the symbol period at a photodetector. During the time–space conversion process, only a portion of the signal energy is converted to a spatial signal. This effect can be accounted for by considering the energy conversion efficiency, and is dependent on x'' [3]. Thus, we can consider the following equivalent system. By substituting $\mu = 2\zeta x''/c$, the time–space processor can be considered as a filter with impulse response $p_\tau(-\mu)$, followed by a gain factor corresponding to the energy conversion efficiency.[2] Then, the equivalent input and output signal of the filter, $r_{\text{in}}(\mu)$ and $r_{\text{out}}(\mu)$, respectively, are related by

$$
r_{\text{out}}(\mu) = \sqrt{\frac{\nu(\mu)}{\alpha_2 \tau^2 \gamma}} r_{\text{in}}(\mu) \otimes p_\tau(-\mu) \tag{6}
$$

where $\nu(\mu)$ is the energy conversion efficiency, which depends on reference pulse energy as well as other parameters of the time–space processor, $\alpha_2 = \int_{-\infty}^{\infty} p_u^2(t)dt$, and γ is a constant. Note that $\alpha_2 \tau^2 \gamma$ in the denominator of (6) is introduced in order to make $\nu(\mu)$ be indeed the energy conversion efficiency, which will be shown explicitly later. Since the width of the pupil function, L, is much wider than D in cases of interest, we will assume from now on that the conversion efficiency is constant within a photodetector size, that is $\nu(\mu) = \nu_m$ for $\mu \in [(m - X_c)T_{\text{ps}} - (\epsilon\tau/2), (m - X_c)T_{\text{ps}} - (\epsilon\tau/2)]$, where $\epsilon = (2\zeta D/c\tau)$ is the normalized (by τ) photodetector size in the μ domain.[3] Finally, the energy incident to the mth photodetector is given by

$$
e_m = \int\limits_{(m-X_c)T_{\text{ps}} - \frac{\epsilon\tau}{2}}^{(m-X_c)T_{\text{ps}} + \frac{\epsilon\tau}{2}} |r_{\text{out}}(\mu)|^2 \, d\mu. \tag{7}
$$

---

[2]μ has dimensions of time and is a mapping of the spatial coordinate x'' back to time.

[3]ϵ is a measure of the detector width when mapped to the time domain and will be shown in the analysis to be an important parameter.

The equivalent input signal, $r_{in}(\mu)$, can be expressed as

$$r_{\text{in}}(\mu) = \sqrt{\frac{GE_0}{\alpha_2\tau}} p_\tau\left(\mu - (d - X_c)T_{\text{ps}}\right) + \sqrt{\frac{GE_0}{\alpha_2\tau}} v(\mu) + n_a(\mu) \quad (8)$$

where $\alpha_2 = \int_{-\infty}^{\infty} p_u^2(t)dt$, $E_0 = \alpha_2\tau P_0$ is the energy of a received ULP, G is the gain of the optical amplifier, and d is the transmitted symbol. According to [1, Prop. 1 and 5, and Lemma 1], the interuser interference $v(t)$ is a zero-mean complex Gaussian process with correlation function

$$R_v(\mu_0; \mu) = E\left\{v(\mu)v^*(\mu + \mu_0)\right\}$$
$$\cong \frac{R_p\left(\frac{\mu_0}{\tau}\right)}{N_{\text{eff}}} \sum_{j=1}^{J-1} \text{sinc}^2\left(\Omega(\mu - \lambda_j)\right) \quad (9)$$

where $R_p(t_0) = (1)/(\alpha_2) \int_{-\infty}^{\infty} p_u(t)p_u(t + t_0)dt$, $N_{\text{eff}} = 1/\alpha_2\tau\Omega$ represents the effective number of spectral CDMA chips contained in the pulse bandwidth, Ω is the chip bandwidth defined in [1], J is the number of users, and λ_j is the time delay of the jth interferer. The approximation follows from the assumptions that $\Omega\tau \ll 1$ and $\Omega|\mu_0| \ll 1$, which are true for most cases of interest. Here we define

$$l_m \triangleq \sum_{j=1}^{J-1} \text{sinc}^2\left(\Omega\left((m - X_c)T_{\text{ps}} - \lambda_j\right)\right) \quad (10)$$

as the equivalent number of interferers at the mth signal location, where the term "equivalent number of interferers" comes from the fact that l_m is the interference power at the mth signal location normalized by the peak interference power caused by a single interferer. The amplifier noise can be modeled as white Gaussian noise in the range of frequency of interest [5]. Thus, $n_a(\mu)$ is modeled as a zero-mean complex white Gaussian process with two-sided spectral density $N_{0,a} = n_{\text{sp}}hf_0(G-1)$ [5], where n_{sp} is the spontaneous emission factor of the amplifier (ideally 1) and h is Planck's constant.

Consider the mth photodetector output. From (6), the signal component, $r_{o,s}(\mu)$, the interuser interference component, $r_{o,i}(\mu)$, and the amplifier noise component, $r_{o,a}(\mu)$, of $r_{\text{out}}(\mu)$ are presented below. The signal component is given by

$$r_{o,s}(\mu) = \frac{1}{\alpha_2\tau}\sqrt{\frac{\nu_m GE_0}{\gamma\tau}} p_\tau\left(\mu - (d - X_c)T_{\text{ps}}\right) \otimes p_\tau(-\mu)$$
$$= \sqrt{\frac{\nu_m GE_0}{\gamma\tau}} R_p\left(\frac{\mu - (d - X_c)T_{\text{ps}}}{\tau}\right)$$
$$\cong \sqrt{\frac{\nu_m GE_0}{\gamma\tau}} R_p\left(\frac{\mu - (m - X_c)T_{\text{ps}}}{\tau}\right)$$
$$\times \delta_K(d - m) \quad (11)$$

where $\delta_K(\cdot)$ is the Kronecker delta function and the last approximation is valid when T_{ps} is sufficiently larger than τ, as shown in [1]. Since the energy contained in $r_{o,s}(\mu)$ is $\nu_m GE_0$, we get $\gamma = 1/\tau \int_{-\infty}^{\infty} R_p^2(t/\tau)dt = \int_{-\infty}^{\infty} R_p^2(t)dt$. The interuser interference component

$$r_{o,i}(\mu) = \frac{1}{\alpha_2\tau}\sqrt{\frac{\nu_m GE_0}{\gamma\tau}} v(\mu) \otimes p_\tau(-\mu) \quad (12)$$

is a zero-mean complex Gaussian random process with correlation function

$$R_{n,i}(\mu_0; m) = E\left\{r_{o,i}(\mu)r_{o,i}^*(\mu + \mu_0)\right\}$$
$$= \frac{\nu_m GE_0}{\gamma\alpha_2^2\tau^3} R_v(\mu_0; \mu) \otimes p_\tau(\mu_0) \otimes p_\tau(\mu_0)$$
$$= \frac{\nu_m GE_0 l_m}{N_{\text{eff}}\alpha_2^2\gamma\tau^3} R_p\left(\frac{\mu_0}{\tau}\right) \otimes p_\tau(-\mu_0) \otimes p_\tau(\mu_0)$$
$$\cong \frac{\nu_m GE_0 l_m}{\alpha_2\gamma\tau N_{\text{eff}}} R_2\left(\frac{\mu_0}{\tau}\right) \quad (13)$$

where $R_2(\mu) \triangleq R_p(\mu) \otimes R_p(\mu)$, and the approximation comes from the assumption $\Omega\tau \ll 1$. Finally, the amplifier noise component

$$r_{o,a}(\mu) = \sqrt{\frac{\nu_m}{\alpha_2\gamma\tau^2}} n_a(\mu) \otimes p_\tau(-\mu) \quad (14)$$

is a zero-mean complex Gaussian random process with correlation function

$$R_{n,a}(\mu_0) = E\left\{r_{o,a}(\mu)r_{o,a}^*(\mu + \mu_0)\right\}$$
$$= \frac{\nu_m N_{0,a}}{\alpha_2\gamma\tau^2} p_\tau(-\mu_0) \otimes p_\tau(\mu_0)$$
$$= \frac{\nu_m N_{0,a}}{\gamma\tau} R_p\left(\frac{\mu_0}{\tau}\right). \quad (15)$$

Let us define $r_{o,n}(\mu) \triangleq r_{o,i}(\mu) + r_{o,a}(\mu)$. Since $r_{o,i}(\mu)$ and $r_{o,a}(\mu)$ are independent, $r_{o,n}(\mu)$ is a zero-mean complex Gaussian process with correlation function $R_n(\mu_0; m) = R_{n,i}(\mu_0; m) + R_{n,a}(\mu_0)$. Then, the mean and variance of the input energy, e_m, to the mth photodetector are given by (see Appendix A)

$$E\{e_m\} \cong \nu_m GE_0 \rho_\epsilon \delta_K(m - d) + \epsilon\tau R_n(0; m) \quad (16)$$
and

$$\text{Var}\{e_m\} \cong \int_{-\frac{\epsilon\tau}{2}}^{\frac{\epsilon\tau}{2}} \int_{-\frac{\epsilon\tau}{2}}^{\frac{\epsilon\tau}{2}} \left(2r_{o,s}(\mu_1)r_{o,s}(\mu_2)R_n(\mu_1 - \mu_2; m)\right.$$
$$\left. \cdot \delta_K(m - d) + R_n^2(\mu_1 - \mu_2; m)\right) d\mu_1 d\mu_2 \quad (17)$$

respectively, where $\rho_\epsilon = 1/\gamma \int_{-\epsilon/2}^{\epsilon/2} R_p^2(\mu)d\mu$.

Additional insight into the statistic of the photodetector input is obtained by using the Gaussian ULP profile, that is, $p_u(\mu) = \exp(-(2\ln 2)\mu^2)$. Then, we get $\alpha_2 = \sqrt{(\pi)/(4\ln 2)}$, $R_p(\mu) = \exp(-(\ln 2)\mu^2)$, $R_2(\mu) = \sqrt{2}\alpha_2 \exp(-(\ln 2/2)\mu^2)$, and $\gamma = \sqrt{(\pi)/(2\ln 2)}$. Thus, we have

$$E\{e_m\} \cong \frac{1}{\epsilon} A_m \Lambda(2\ln 2, 0, 0; \epsilon)\delta_K(m - d)$$
$$+ \epsilon(B_m + C_m) \quad (18)$$
and

$$\text{Var}\{e_m\} \cong 2A_m\left(B_m\Lambda\left(\frac{3\ln 2}{2}, \ln 2, \frac{3\ln 2}{2}; \epsilon\right)\right.$$
$$+ C_m\Lambda(2\ln 2, 2\ln 2, 2\ln 2; \epsilon)))\delta_K(m - d)$$
$$+ ((B_m^2\Lambda(\ln 2, 2\ln 2, \ln 2; \epsilon)$$
$$+ 2B_m C_m\Lambda\left(\frac{3\ln 2}{2}, 3\ln 2, \frac{3\ln 2}{2}; \epsilon\right)$$
$$\left. + C_m^2\Lambda(2\ln 2, 4\ln 2, 2\ln 2; \epsilon))\right) \quad (19)$$

where $A_m = (\nu_m G E_0)/(\gamma)$, $B_m = (\sqrt{2}\nu_m G E_0 l_m)/(\gamma N_{\text{eff}})$, $C_m = (\nu_m n_{sp} h f (G-1))/(\gamma)$

$$
\begin{aligned}
\Lambda(c_1, c_2, c_3; \epsilon) &\triangleq \int_{-\frac{\epsilon}{2}}^{\frac{\epsilon}{2}} \int_{-\frac{\epsilon}{2}}^{\frac{\epsilon}{2}} \exp(-c_1\mu_1^2 + c_2\mu_1\mu_2 - c_3\mu_2^2)d\mu_1 d\mu_2 \\
&= \sqrt{\frac{\pi}{c_1}} \int_{-\frac{\epsilon}{2}}^{\frac{\epsilon}{2}} \left[Q\left(-\sqrt{\frac{c_1}{2}}\epsilon - \frac{c_2\mu}{\sqrt{2c_1}}\right) \right. \\
&\qquad\qquad \left. - Q\left(\sqrt{\frac{c_1}{2}}\epsilon - \frac{c_2\mu}{\sqrt{2c_1}}\right) \right] \\
&\qquad \times \exp(-c_4\mu^2)d\mu
\end{aligned}
\tag{20}
$$

$Q(x) = (1)/(\sqrt{2\pi}) \int_x^\infty \exp(-t^2/2)dt$, $c_1 > 0$, and $c_4 = (4c_1 c_3 - c_2^2)/(4c_1)$.

Now, define the input SNR of the dth photodetector as

$$
\text{SNR}_{in,d} = \frac{(E\{e_d\} - \epsilon\tau R_n(0; d))^2}{\text{Var}\{e_d\}}
\tag{21}
$$

where $E\{e_d\} - \epsilon\tau R_n(0; d)$ is the component of e_d due to the signal. As can be seen in (11), (13), and (15), the input SNR depends on E_0 and is almost independent of G when G is large. When E_0 is large, the interuser interference dominates the amplifier noise. However, the peak power of the transmitted signal should be small enough not to introduce nonlinear distortion in the optical fiber. Recently, it was shown in [6] that an ULP with 40 w peak power and 400 fs full-width half-maximum (FWHM) duration can be successfully transmitted over a 2.5 km precompensated fiber link. In ULP-CDMA systems, the CDMA spreading reduces the peak power of the transmitted signal by the factor of N_{eff}, in an average sense. On the other hand, multiple users can be concurrent, and thus increase the peak power. Finally, the peak power requirement for narrower ULPs is more restrictive. For a 100 fs ULP, we assume that it is enough to keep the average peak power, averaged over random time delays and random signature code ensemble, below a tenth of the result in [6] as a rule of thumb. Then, the maximum allowable value of E_0 is about 40 pJ.

In Fig. 4, the input SNR is plotted as a function of ϵ, when a Gaussian pulse profile is used and E_0 is 1 fJ, 0.1 pJ, and 10 pJ, respectively. Here we set the conversion efficiency and the amplifier gain to 0.1% and 30 dB, respectively, and the effective number of interferers is the average number of interferers, $(J-1)/(T_s\Omega) = (\alpha_2 N_{\text{eff}}(J-1)\tau)/(T_s)$, where $J = 1000$, $\tau = 100$ fs, and $T_s = 10$ ns. We see clearly that the input SNR decreases as ϵ increases. The maximum input SNR is obtained when $\epsilon \to 0$ and is given by $10\log_{10}((A_d^2)/((2A_d + B_d + C_d)(B_d + C_d)))$. In this case, the input energy follows a noncentral chi-square distribution with two degrees of freedom. The result also shows that the amplifier noise is negligible when $E_0 \geq 0.1$ pJ, with the given parameters.

Now, consider the detector noise. We assume that we use an avalanche photodetector (APD) array. Let i_m, G_a, i_{dark}, η, and ϱ be the photocurrent at the mth detector, the APD gain, the dark current, the APD quantum efficiency, and the excess noise
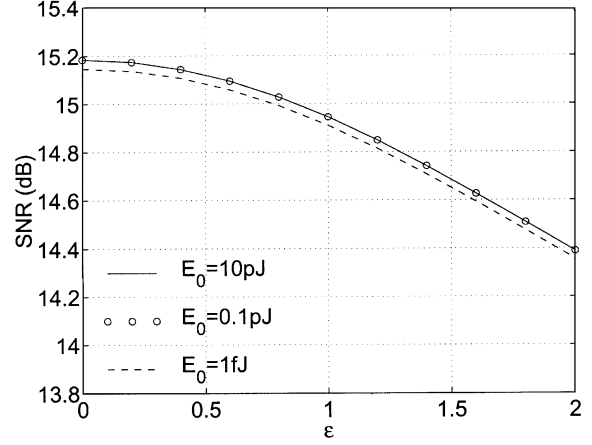

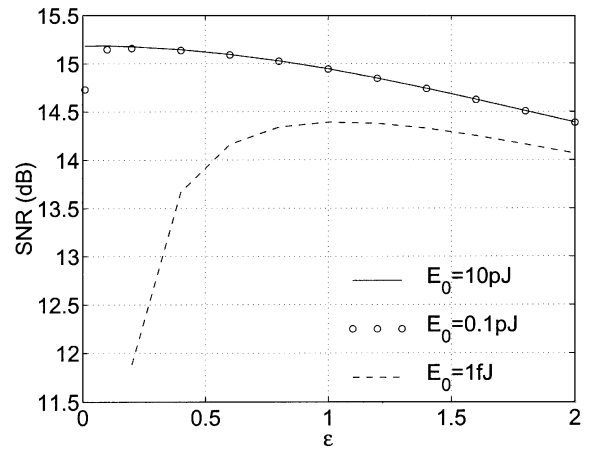Fig. 4. Input SNR to the dth photodetector.

Fig. 5. Output SNR from the dth photodetector.

factor, respectively. Using the input power-generated current relation of an APD [7], the mean and variance of i_d are as follows:

$$
E\{i_d\} = G_a\left(RT_s^{-1}E\{e_d\} + i_{\text{dark}}\right)
\tag{22}
$$

and

$$
\begin{aligned}
\text{Var}\{i_d\} &= qG_a^{2+\varrho}\left(RT_s^{-1}E\{e_d\} + i_{\text{dark}}\right)B_e + \frac{2k_B T_r}{R_L}B_e \\
&\quad + G_a^2 R^2 T_s^{-2}\text{Var}\{e_d\}
\end{aligned}
\tag{23}
$$

where $R = (q\eta)/(hf_0)$ is the receiver responsivity, q is the electron charge, B_e is the electrical bandwidth (equal to T_s^{-1}), k_B is the Boltzman constant, T_r is the receiver temperature, and R_L is the load resistance. Then, the output SNR from the dth photodetector may be defined as

$$
\text{SNR}_{out,d} = \frac{G_a^2 R^2 T_s^{-2}(E\{e_d\} - \epsilon\tau R_n(0; d))^2}{\text{Var}\{i_d\}}.
\tag{24}
$$

In Fig. 5, the output SNRs are plotted for $E_0 = 10$ pJ, 0.1 PJ, and 1 fJ, respectively, when $G_a = 100$, $\varrho = 0.35$, $i_{\text{dark}} = 0.1$ nA, $R_L = 100$ Ω, and $\eta = 0.75$, which are typically used parameters for Si APD. We can see that when $E_0 \geq 0.1$ pJ and $\epsilon \geq 0.1$, the interference noise dominates both the amplifier noise and detector noise with the given parameters.

From these results, we see that the amplifier and detector noise can be ignored for reasonable parameters and signal en-

ergy. In addition, the desired physical size of the photodetectors is typically smaller than the pulse width (that is, $\epsilon < 1$). Since the bandwidth-time (BT) product of the input energy, e_m, is small (<1), e_m can be modeled as a (noncentral) chi-square random variable with two degrees of freedom, which indicates that the results shown in [1] are still valid over the range of bit-error probabilities of interest (that is, when the number of interferers is not too small) with reasonable parameters and signal energy levels. However, in a very low signal energy regime, amplifier and detector noise are not negligible. In addition, the detector size should be large enough (that is, $\epsilon > 1$) to receive a large amount of signal energy to combat detector noise. In this case, the input SNR is reduced (as shown in Fig. 4) and the BT product of e_m becomes comparable to one. When the BT product is large, e_m can be modeled as a (noncentral) chi-square random variable with $2\text{BT}+1$ degrees of freedom [8], [9]. However, since the BT product is comparable to one, eigenfunction expansion methods [10], [11] should be adopted to characterize the probability density function (pdf) of e_m. In addition, detector noise becomes significant. Thus, the results shown in [1] will deviate from actual performance measurements.

IV. DESIGN ISSUES FOR SYSTEM PARAMETERS

Due to the broadband nature of ULPs, ULP-CDMA systems are vulnerable to the dispersion of the optical fiber. Dispersion compensation techniques by matching fibers with opposite dispersion signs can be applied to circumvent group velocity dispersion, the primary contributor to dispersion. However, for ULPs, the higher order dispersion terms must be included. These dispersion orders are harder to compensate by optical fiber combinations and will result in a residual dispersion term. A recent example of short pulse propagation in dispersion-managed fiber compensations has demonstrated 400 fs pulse propagation over 60 km fiber with the pulse width increasing to 600 fs [12]. By combining an adaptive spectral filter to the dispersion-managed fiber, higher order dispersion terms can be nearly eliminated, as demonstrated in a 480 fs pulse transmission over 3 km with pulse broadening of only 10 fs [13], and recently a 400 fs transmission over 10 km with 5 fs broadening [14].

In the proposed PPM/ULP-CDMA system, the pulse separation in the PPM format, T_{ps}, should be set large enough to prevent a signal component from contributing to the neighboring locations. Thus, a design tradeoff is established in the selection of pulse duration; short pulses yield better performance, in principle, but they are more susceptible to pulse broadening due to dispersion, resulting in an increase of T_{ps}, which reduces the actual performance, since fewer pulse positions are allowed in the receiver's time window. This tradeoff signifies the importance of combating dispersion for achieving high throughput. A dispersion compensation and receiver synchronization technique, by transmitting a reference pulse through the system, is illustrated below.

For time-to-space conversion to occur, a properly-timed reference pulse must be provided. A local reference pulse source, locked to the transmitter laser, is a possible, yet difficult, solution, since the synchronization has to be better than the pulse

duration (i.e., in the femtosecond range). We envisage an alternate possibility, where a reference pulse is transmitted through the optical fiber with delay t_0 relative to the data pulse. At the receiver, the incoming signal is divided into two branches having unequal delays, such that the reference pulse and the data pulse enter the processor at the same time. Using this scheme, the optical input channel containing the reference pulse carries also an interference component. In addition, there is 3 dB signal energy loss due to the division of the incoming beam. However, with reasonable signal energy and large number of users, we can assume that other users' interference is the main source of performance degradation and the interference is also 3 dB attenuated by the division of incoming beam. We analyze the time-to-space converted signal in the presence of interference with the reference pulse by ignoring the 3 dB attenuation effect.

As before, the detection process occurs after the CDMA despreading filter has recompressed the desired users' data and reference pulses back to an ULP. We assume that the reference pulse is delayed by t_0 relative to the center position of the PPM format, such that at the input to the processor (after path-length correction), $r_{\text{ref}}(t) = \sqrt{P_0}p_\tau(t) + \sqrt{P_0}v(t + t_0)$ and $s(t)$ remains unchanged. The ultrafast waveforms are incident on the diffraction gratings at the input plane of the SPD, generating U_1 and U_2, defined in (1) and (2), respectively. The interaction of the waves will have four components: 1) data pulse and reference pulse; 2) interference concurrent with data pulse and reference pulse; 3) interference concurrent with reference pulse and data pulse; and 4) interference concurrent with data pulse and interference concurrent with reference pulse. Since we are typically operating in the high signal-to-interference ratio regime for low bit-error probability, we can ignore the effect of the mutual interaction of interferences, 4). Following the same derivation for components 1)–3), the output field is given by

$$
\begin{aligned}
U_{\text{out}}(x''; t) \propto \exp(j2\omega_0 t) \Bigg\{ & \Bigg(\Bigg(p_\tau \left(\frac{2\zeta x''}{c} - (d - X_c)T_{\text{ps}} \right) \\
& + v \left(\frac{2\zeta x''}{c} \right) \Bigg) \otimes p_\tau \left(-\frac{2\zeta x''}{c} \right) \Bigg) \\
& \times w \left(-\frac{ct}{\zeta L} \right) w \left(\frac{ct}{\zeta L} - \frac{2x''}{L} \right) \\
& + \left(v \left(t_0 + (d - X_c)T_{\text{ps}} - \frac{2\zeta x''}{c} \right) \right. \\
& \otimes p_\tau \left(\frac{2\zeta x''}{c} \right) \Bigg) w \left(-\frac{ct}{\zeta L} + \frac{c}{\zeta L} \right. \\
& \times (d - X_c)T_{\text{ps}} - \frac{2x''}{L} \Bigg) w \left(\frac{ct}{\zeta L} \right. \\
& \left. - \frac{c}{\zeta L}(d - X_c)T_{\text{ps}} \right) \Bigg\}.
\end{aligned}
\tag{25}
$$

The stationary output field components carry the time-to-space converted information. It consists of the signal pulse, the accompanying interference, and the interference accompanying the reference pulse. Note that the latter is reversed in spatial coordinate, relative to the other signals. The temporal dynamics of the fields, due to the spatial pupil modes, are irrelevant in the detection process due to the long integration time of the detectors. Since $v(\cdot)$ is a Gaussian process and t_0 can be made suf-

ficiently large (e.g., several times of $1/\Omega$) such that there is no correlation between the interference components, the sum of the two interference components is Gaussian, and its variance is the sum of that of each interference component, resulting in worse performance, while eliminating the synchronization problem. Roughly speaking, the aggregate throughput is one-fourth of that expected by assuming a perfect reference pulse, since both the number of interference pulses and the probability that an interference pulse is concurrent with the desired one are doubled. To reduce the performance degradation, we can transmit the signal and reference pulses with two orthogonal polarization states via a polarization preserving fiber. In this case, only the interfering probability is doubled, and the performance degradation factor is roughly a factor of two. Considering the intensity noise, the situation could be worse. The intensity noise is on the signal pulse as well as on the reference pulse. In addition, the intensity noise on the signal pulse could be correlated or uncorrelated to that on the reference pulse, depending on how one obtains the reference pulse. Interferers' pulses also carry intensity noise. Although an exact analysis including intensity noise is very complex and is beyond the scope of this paper, we can assume that a typical pulse-to-pulse energy variation is about 1%. Thus, although it reduces the actual aggregate throughput, it would not degrade the performance seriously.

An additional advantage of using a pulse that has traveled through the optical fiber for the reference pulse is that the pulse carries information about the fiber channel. The dispersion that will affect the data pulse also affects the reference pulse. When the time–space processor is used in a communication system where both the reference pulse and the signal pulse traverse the same optical channel, all the odd-order dispersion terms are automatically cancelled [15]. On the other hand, the even-order terms are doubled in magnitude. Since the second-order dispersion is the main source of signal distortion in uncompensated fiber propagation, this could have a detrimental effect. However, the time–space processor can compensate for second-order dispersion by displacing the output plane of the processor. Since the second-order dispersion is quadratic in the temporal frequency domain, the converted spatial information contains quadratic phase. By free-space propagation, the spatial quadratic phase is compensated, resulting in a signal that is distorted by the fourth and higher even orders. These orders are very weak and do not contribute significantly to the dispersion.

In [1], it was shown that the performance of the proposed system depends largely on three parameters: the ULP duration τ; the chip bandwidth Ω; and the number of possible signal positions M. In addition, the pulse separation, T_{ps}, should be selected to ensure signal orthogonality. In the remaining portion of this section, practical ranges of the parameters are briefly discussed.

First, consider the minimum pulse separation time, T_{ps}, that ensures that the detected waveforms are sufficiently orthogonal. Here, we assume that the fiber dispersion effect is eliminated by applying a good dispersion compensation technique. Since some pulse shapes, e.g., Gaussian, are not limited in the time domain, we wish to establish the required distance between pulses such that the received signal in adjacent channels is sufficiently small. By using a Gaussian pulse profile, we can calculate the

signal component energy at the desired and adjacent locations from (7) and (11). When $\epsilon = 1$, we see that $T_{\mathrm{ps}} \geq 2\tau$ assures the fractional energy spilling to a neighboring detector is less than 1%. Typically, ϵ should be less than one in the moderate-to-high signal energy regimes, as shown in Section III. In this case, the fractional energy is typically reduced further.

The advent of erbium-doped, fiber-based ultrashort pulse lasers provide an ideal source for ULP communications, as the oscillation frequency of these lasers coincides with the desired communication band (center wavelength 1550 nm), and the robust fiber laser can be easily and efficiently connected to the optical network. Such lasers, based on additive-pulse mode locking, operating with $\tau = 90$ fs, at 40 MHz repetition $(T_s = 25 \text{ ns})$, 2.25 nJ energy per pulse, and at wavelength 1550 nm, have been demonstrated in [16]. Lasers with higher repetition rates of 10 GHz $(T_s = 0.1 \text{ ns})$ have also been demonstrated with excellent jitter characteristics in [17].

The time window of the receiver is required to span the duration of the all possible symbols, MT_{ps}. Using the time-to-space mapping, the duration corresponds to a spatial width of $cMT_{\mathrm{ps}}/2\zeta$. We seek the width of the spatial mode of the beam, L, to cover this time window. Assuming that the detected values can be as low as 10% at the window extremes, relative to those at the center of the window, and $T_{\mathrm{ps}} = 2\tau$, then the relationship $cM\tau/\zeta L = \sqrt{\ln 10}$ is established. Theoretically, we can increase L to accommodate any M. However, increasing L decreases the efficiency of the time–space processor, as well as introducing a packaging problem as the system size increases. A reasonable system may accommodate a time window on the order of 5–50 ps, allowing M up to the hundreds.

Finally, consider the spectral chip bandwidth, Ω. The limiting factor on the possible spectral chip bandwidth that can be employed is the spectral resolution of the CDMA encoding spectral filter. The spectral resolution can be improved by increasing the beam size. However, a larger beam would require larger gratings and lenses, resulting in a bulky system that is more prone to stability problems. A recently demonstrated guided-wave optical implementation, based on arrayed waveguide grating, achieved an impressive resolution of 10 GHz in a small, robust package [18]. Thus, time-spread waveforms will emerge with typical durations on the order of 100 ps. This excellent performance is attributed to the array of 340 waveguide delay lines.

V. TWO MODIFIED SCHEMES

As discussed in [1], we can improve the performance of the hybrid PPM/ULP-CDMA system by reducing τ, increasing M, and/or increasing N_{eff}. In Section IV, however, it was shown that there are some practical limitations on the system parameters. In this section, two modified schemes are proposed to overcome such difficulties and enhance the performance of the hybrid PPM/ULP-CDMA system.

A. Multiple-Bit Transmission Scheme

The performance of the PPM/ULP-CDMA system depends largely on N_{eff}. As mentioned in Section IV, however, it is difficult to increase N_{eff} beyond a certain degree. Thus, only a
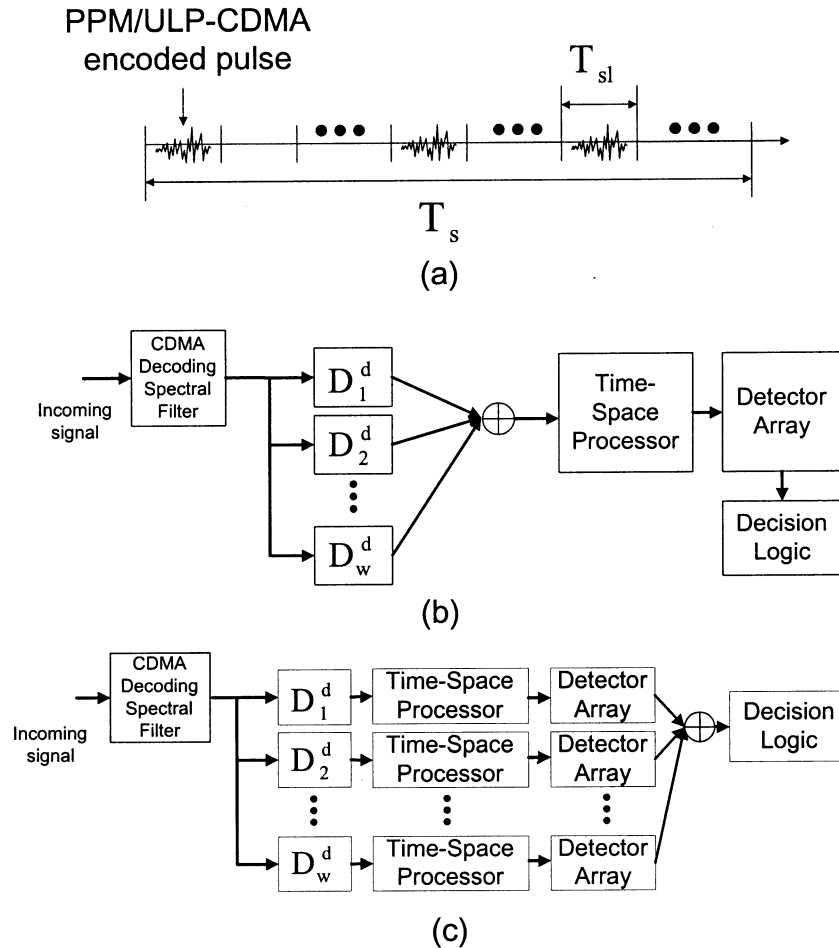
Fig. 6.   Schematics of the MPT scheme. (a) Transmitted signal pattern. (b) Coherent combining receiver structure. (c) Intensity combining receiver structure.

small portion of the symbol period is occupied by the transmitted signal, and thus, for a large percentage of the time, no signal is being sent. As a way to use this unexploited resource, a multiple-pulse transmission (MPT) technique is considered. The basic idea of the MPT scheme is to use a repetition code of length w (with peak power of each pulse P_0/w) in each symbol period to enable diversity reception, as shown in Fig. 6(a). However, we cannot get a performance gain if we send them periodically, because a pulse of an interferer that is concurrent with any pulse of the desired user implies that all pulses of the desired user are corrupted by that interferer. As a remedy, we use optical orthogonal codes (OOC) [19] to specify the multiple pulse positions. If we assign a different OOC to each user, an interferer (with w interfering pulses) can, at most, corrupt one of the w pulses of the desired user. However, the number of available OOCs is bounded by $\beta = \lfloor (F-1)/w(w-1) \rfloor$ [19], where $\lfloor a \rfloor$ denotes the greatest integer not exceeding a, $F = T_s/T_{sl}$, and $T_{sl} \geq 2/\Omega + (M-1)T_{ps}$ is the duration of a slot in which an M-ary PPM symbol can reside. For example, let $T_{sl} = 50\text{ps}$ and $T_s = 10\text{ns}$. Then, we get about 100 OOCs when $w = 2$, and 10 OOCs when $w = 5$. Since there are not a sufficient number of OOCs for all users, the users are divided into as many groups as available OOCs, and an OOC is assigned to all users in a group. We can also use OOCs with correlation value bounded by two in order to increase the number of OOCs. Note that the number of users in the MPT scheme is not limited by the number of OOCs.

However, for a given number of users, the number of users in a group is inversely proportional to the number of OOCs, and the probability that all w pulses of the desired user are corrupted by an interferer decreases as the number of users in a group decreases. Thus, we can reduce the impulsiveness of interference by using well-designed OOCs with correlation value bounded by two. However, the probability distribution of "hit(s)" of an OOC with correlation value bounded by two depends on the code construction of the OOC, and the actual code construction and optimization is beyond the scope of this paper. Therefore, we will focus on the OOC with correlation value bounded by one in the sequel.

Now, consider receiver structures for the MPT scheme. First, consider the coherent combining of the received signal at the receiver, as shown in Fig. 6(b). Here, D_i^j represents the ith repetitive pulse position (in time) of the OOC of the jth user. Let $l_d = \sum_{i=1}^{w} l_{d,i}$ and $l_r = \sum_{i=1}^{w} l_{r,i}$, where $l_{d,i}$ and $l_{r,i}$ are the effective numbers of interferers at the desired and the rT_{ps}-apart PPM signal locations in the ith repetitive pulse position, respectively. Then, after coherently combining w pulses, the pairwise error probability (PEP) ([1, eq. (18)]), conditioned on $l_d + l_r$, can be modified as

$$\Pr\{I_d < I_r | l_d + l_r = l\} = \frac{1}{2}\exp\left(-\frac{w^2 N_{\text{eff}}}{l}\right), \qquad l > 0. \tag{26}$$

The u^2 term in the numerator of the exponent of (26) arises as follows. From [1, eq. (16)–(18)], the variance of the interference is given by $P_0(l_d+l_r)/N_{\text{eff}}$. Also, the signal power is $w^2 P_0$ due to the coherent combining. Thus, the signal-to-interference ratio becomes $w^2 N_{\text{eff}}/(l_d + l_r)$. On the other hand, the probability $\Pr\{l_d + l_r = l\}$ should be modified also. Since the crosscorrelations of the OOCs are bounded by one, at most, one encoded pulse of an interferer can be concurrent with the desired user's pulses. Since each user transmits w encoded pulses, and the time window of interest of the desired user increases to w times that in the conventional hybrid PPM/ULP-CDMA system (that is, w pulses of the desired user are combined), the probability that one encoded pulse of an interferer is within the time window of interest of the desired user is w^2 times that in the conventional scheme (here, the effect of insufficient OOCs is ignored for simplicity). Then, [1, eq. (20)] can be modified as

$$P(r,k) = \binom{J-1}{k}\left(\frac{2w^2 T}{T_s}\right)^k \left(1 - \frac{2w^2 T}{T_s}\right)^{J-k-1}. \quad (27)$$

Note that the time interval $[-T, T]$ is used instead of $[-T, T + rT_{\text{ps}}]$ for simplicity. This can be justified from the facts that T_{ps} is typically much smaller than T and that, as seen in [1, Fig. 5], the amount of interference caused by an interferer is relatively small when the time delay of the interferer is within $[-T, -T + rT_{\text{ps}}/2]$ or $[T + rT_{\text{ps}}/2, T + rT_{\text{ps}}]$. Since $T = 1/\Omega$ and $N_{\text{eff}} = 1/\alpha_2\Omega\tau$, (26) and (27) are equivalent to those of the conventional hybrid PPM/ULP-CDMA system with the spectral chip bandwidth Ω/w^2, which means the effective number of chips increased by a factor of w^2. Thus, from [1, eqs. (21)–(25)], it is seen that the performance of the MPT/coherent combining is equivalent to that of the conventional hybrid PPM/ULP-CDMA system with effective number of chips increased by a factor of w^2, which implies the performance of the hybrid PPM/ULP-CDMA system is improved by the MPT/coherent combining scheme. However, the implementation of the coherent combining receiver is quite difficult, due to the very high frequency of the optical carrier.

In Fig. 6(c), an intensity combining scheme is shown. The intensities detected by the detector arrays are combined and compared. Then, the largest one is selected. Although the intensity combining is inferior to the coherent combining, this scheme may be preferred, since it can be easily implemented. Let $I_{d,i}$ and $I_{r,i}$ be the intensities detected at the desired and rT_{ps}-apart PPM signal locations of the ith repetitive pulse position. Then, after combining, we get $I_d = \sum_{i=1}^{w} I_{d,i}$ and $I_r = \sum_{i=1}^{w} I_{r,i}$. Since the interference, conditioned on the time delays of the interferers, is Gaussian, the pdf of I_r, conditioned on $l_{r,v}$, $v = 1, \cdots, w$, is given by [20, p. 802]

$$f_r(I_r|l_{r,1},\cdots,l_{r,w}) = \sum_{v=1}^{w} \frac{wN_{\text{eff}}\Pi_v}{P_0 l_{r,v}} \exp\left(-\frac{wN_{\text{eff}} I_r}{P_0 l_{r,v}}\right) \quad (28)$$

where $\Pi_v = \prod_{i=1, i\neq v}^{w}(l_{r,v})/(l_{r,v} - l_{r,i})$. Thus, we have

$$\Pr\{I_r > x|l_{r,1},\cdots,l_{r,w}\} = \sum_{v=1}^{w} \Pi_v \exp\left(-\frac{wN_{\text{eff}} x}{P_0 l_{r,v}}\right). \quad (29)$$

On the other hand, I_d, conditioned on $l_{d,1},\cdots,l_{d,w}$, is the sum of independent noncentral chi-square random variables, each
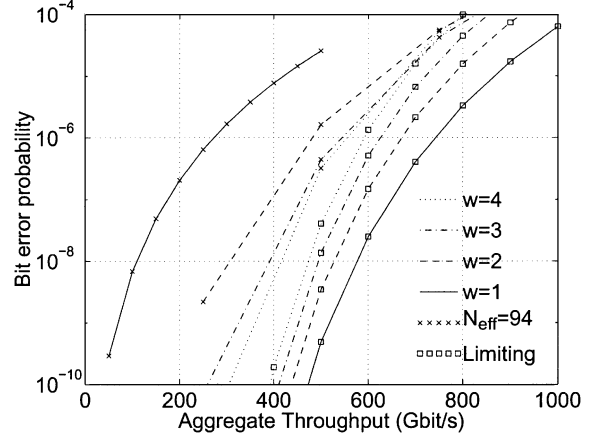

Fig. 7. Bit-error probabilities of the MPT scheme when $\tau = 200$ fs and $M = 32$.

with two degrees of freedom. From the moment generating function (MGF) of a noncentral chi-square random variable given in [20, p. 44], the MGF of I_d is given by

$$\Psi_{I_d|l_{d,1},\cdots,l_{d,w}}(s) = \prod_{q=1}^{w}\left(\frac{\exp\left(\frac{sP_0}{w - \frac{sP_0 l_{d,q}}{N_{\text{eff}}}}\right)}{1 - \frac{sP_0 l_{d,q}}{wN_{\text{eff}}}}\right). \quad (30)$$

Then, the conditional PEP is

$$\begin{aligned}
&\Pr\{I_d < I_r|l_{r,1},\cdots,l_{r,w}, l_{d,1}\cdots,l_{d,w}\}\\
&= \sum_{v=1}^{w}\Pi_v E\left\{\exp\left(-\frac{wN_{\text{eff}} I_d}{P_0 l_{r,v}}\right)\bigg| l_{r,1},\cdots,l_{r,w}, l_{d,1},\right.\\
&\qquad\qquad\qquad\qquad\qquad\qquad \cdots, l_{d,w}\Big\}\\
&= \sum_{v=1}^{w}\Pi_v \Psi_{I_d|l_{d,1},\cdots,l_{d,w}}\left(-\frac{wN_{\text{eff}}}{P_0 l_{r,v}}\right)\\
&= \sum_{v=1}^{w}\Pi_v \prod_{q=1}^{w}\frac{l_{r,v}}{l_{r,v}+l_{d,q}}\exp\left(-\frac{N_{\text{eff}}}{l_{r,v}+l_{d,q}}\right). \quad (31)
\end{aligned}$$

The pairwise probability is obtained by taking the expectation of (31) over $l_{d,1},\cdots,l_{d,w}, l_{r,1},\cdots,l_{r,w}$, or equivalently, over the time delays. In Fig. 7, the union bounds of bit-error probability of the MPT schemes are plotted for $N_{\text{eff}} = 94$ and the limiting case when $\tau = 200$ fs and $M = 32$. To evaluate the PEP, the numerical method used in [1] is employed with modification as shown in Appendix B. From the results, it is seen that we can improve the performance of the hybrid PPM/ULP-CDMA system by employing the MPT scheme when N_{eff} is small and P_{req} is low. Now, consider the limiting case where N_{eff} is sufficiently large. In this case, interference can be considered as a stationary Gaussian process with variance $2\sigma^2 = (((J-1)P_0)/(wN_{\text{eff}}))((w)/(T_s\Omega)) = (\alpha_2(J-1)\tau P_0)/(T_s)$ by invoking the central limit theorem. Then, the PEP is given by [20, p. 686]

$$\Pr\{I_d < I_r\} = \frac{1}{2^{2w-1}}\exp\left(-\frac{P_0}{4\sigma^2}\right)\sum_{n=0}^{w-1}C(w,n)\left(\frac{P_0}{4\sigma^2}\right)^n \quad (32)$$
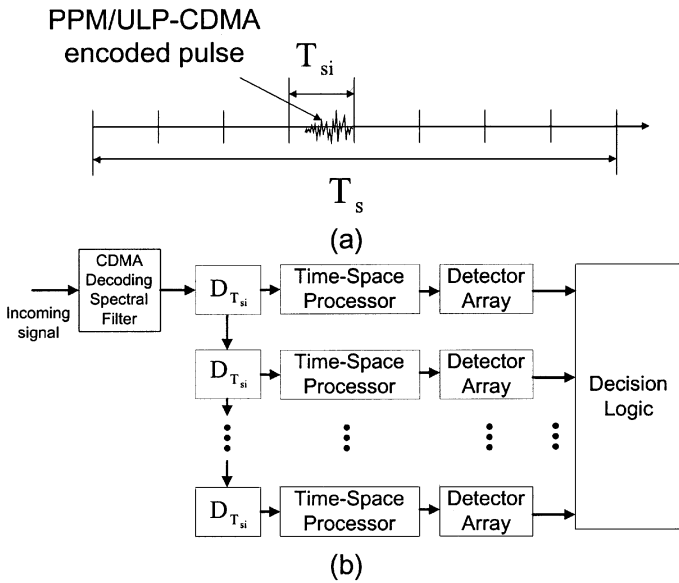
PPM/ULP-CDMA
encoded pulse

(a)

(b)

Fig. 8. Schematics of the ST scheme. (a) Transmitted signal pattern. (b) Receiver structure.

Fig. 9. Symbol-error probabilities of the ST scheme when $\tau = 200$ fs and $M = 32$.

where $C(w, n) \triangleq 1/n! \sum_{m=0}^{w-n-1} \binom{2w-1}{m}$. As seen in Fig. 7, the PEP now increases as w increases, which comes from the noncoherent combining loss. Although the limiting performance gets worse as w increases, the actual performance (with fixed N_{eff}) gets closer to the limiting one as w increases, because the interference gets closer to a stationary Gaussian process as the number of interfering pulses increases. From Fig. 7, we can enhance the performance of the hybrid PPM/ULP-CDMA system with $\tau = 200$ fs, $M = 32$, and $N_{\text{eff}} = 94$ by using the MPT scheme and increasing w up to four at 10^{-6} bit-error probability.

The additional complexity in a transmitter required for the MPT scheme is an optical divider with delay lines. In a receiver, as many pairs of time–space processors and photodetector arrays as the number of pulses in a symbol may be required. However, we can implement a receiver with one pair of time–space processor and photodetector array with a timing circuit when the symbol rate is much slower than the electrical circuit speed.

B. Selective Transmission Scheme

Another important parameter determining the performance of the hybrid PPM/ULP-CDMA systems is the number M of PPM symbols. As discussed in Section IV, however, M is determined by the size of the time window of the time–space processor. To overcome the limitation on M, a selective transmission (ST) scheme is suggested in Fig. 8. Here, the symbol period T_s is divided into w intervals with $T_{si} = T_s/w$, and $\log_2(Mw)$ bits are encoded into a symbol, where $\log_2 w$ bits select one of the w clusters in which the M-ary PPM symbol is transmitted. Then, the signal location with the largest intensity among the Mw possible locations is selected at the receiver. In addition to the enlarged signal set, the ST scheme shuffles the transmission time according to the $\log_2 w$ bits of the information symbol, which implies the interference profiles during different symbol periods are likely to differ, so that the correlation between the bit-error probabilities in different symbol periods is alleviated. Note that
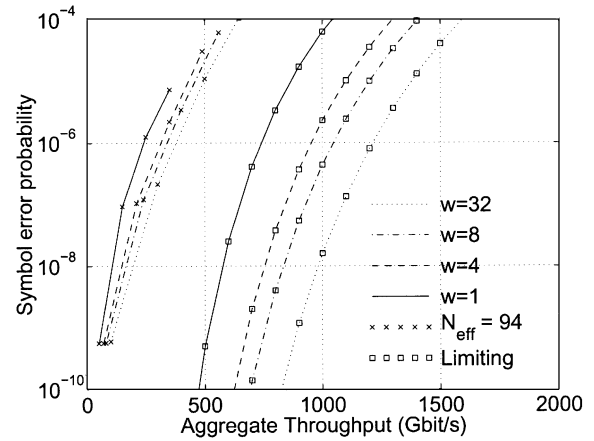
this effect becomes more beneficial when an error-correcting code is employed.

Now, consider the performance of the ST scheme. Since each user transmits only one pulse in a symbol period, the PEP among the adjacent M symbols is identical to that investigated in [1]. On the other hand, the PEP between symbols in different clusters is obtained as follows. Since the separation of the two signal locations is large, an interferer corrupting one signal position can rarely affect the other one at the same time. Since the conditional PEP given in [1], and repeated in this paper as (C-1), still holds, we can apply the same numerical techniques as in [1]. Then, the union bound of the symbol-error probability (or bit-error probability) is obtained from the PEPs (see Appendix C). In Fig. 9, the union bounds of symbol-error probability of the ST scheme are plotted for $N_{\text{eff}} = 94$ and the limiting case when $\tau = 200$ fs and $M = 32$. From the result, we see that we can improve the aggregate throughput with the ST scheme. Although it is not clearly seen in Fig. 9, the aggregate throughput increases nearly proportional to $\log_2(Mw)/\log_2(M) = 1 + \log_M(w)$, except for the $w = 32$ case. This result is due to the fact that the PEP between symbols in different clusters is much smaller than that between symbols in the same cluster, so that the second term in the right-hand side of (C-4) is negligible when w is small. The unequal pairwise error characteristic of the ST scheme may be useful in some applications where information and redundant bits have different significance, such as with a turbo code [21]. In these cases, we may encode bits into a PPM symbol by using more significant bits to select a cluster and less significant bits to select a position in the cluster.

As w increases, the symbol-error probability increases. However, we can still get higher aggregate throughput (although less than linear improvement) at a given symbol-error probability (or bit-error probability) by increasing w. When N_{eff} and J are sufficiently large, the performance of the ST scheme can be obtained from [1, Prop. 7 and Fig. 9] by substituting Mw for M, which shows improvement of aggregate throughput by increasing $\log_2(Mw)$.

Similar to the MPT scheme, the additional complexity in a transmitter using the ST scheme is the additional delay lines and a selecting circuit. For the receiver, we may again use as many pairs of time–space processors and photodetector arrays as the

number of clusters, resulting in roughly linear increase in the receiver complexity. However, we can also implement the receiver with one pair of time–space processor and photodetector array with a timing circuit when the symbol rate is low. In this case, we can improve the performance of the proposed system with only slight additional complexity for both transmitter and receiver.

VI. CONCLUDING REMARK

In this paper, a receiver for the proposed hybrid PPM/ULP-CDMA system using the time–space processor was proposed and investigated. The high resolution time-to-space conversion by the time–space processor enabled detection of the proposed PPM format with very small symbol separation. Some nonideal effects of the time–space processor, including the reference pulse realization, as well as amplifier noise, detector noise, fiber dispersion, and nonlinear distortion in the fiber, were discussed. Also, the system parameters, such as the ULP duration, the ULP repetition time, the spectral chip bandwidth, the number of PPM symbols, and symbol separation of the PPM format, were discussed relative to the current state-of-the-art technology. The performance analysis on the proposed hybrid PPM/ULP-CDMA system with such nonideal effects showed that the results provided in [1] were still valid (with aggregate throughput modification corresponding to the specific reference pulse realization method as discussed in Section IV), for reasonable values of the system parameters, when used for short distance data networks, such as local area networks, where fiber attenuation was negligible and fiber dispersion could be almost compensated with current state-of-the-art technology.

To enhance the performance of the proposed system beyond the physical limit of the system parameters, the MPT and ST schemes were proposed and investigated. It was shown that we could improve the performance of the hybrid PPM/ULP-CDMA system by employing either the MPT or ST schemes. In effect, the MPT scheme increased the effective number of chips, and the ST scheme increased the number of possible symbols in PPM format, both resulting in improved performances at the cost of additional complexity. In particular, the ST scheme can provide improvement in aggregate throughput, nearly proportional to the logarithm of the number of clusters in the PPM format, as well as an additional advantage of interference randomizing and unequal error protection, which might be useful when a channel-coding scheme is applied.

APPENDIX A

DERIVATIONS OF (16) AND (17)

Let us denote $r_{o,n}(\mu) = n_r(\mu) + jn_i(\mu)$. Since the autocorrelation functions $R_{n,i}(\mu; m)$ and $R_{n,a}(\mu)$ are real, $n_r(\mu)$ and $n_i(\mu)$ are independent Gaussian processes with zero mean and identical autocorrelation function $1/2R_n(\mu_0; m)$. Then we have

$$
\begin{aligned}
E\left\{|r_{\text{out}}(\mu)|^2\right\} &= r_{o,s}^2(\mu) + 2r_{o,s}(\mu)E\left\{n_r(\mu)\right\} \\
&\quad + E\left\{n_r^2(\mu) + n_i^2(\mu)\right\} \\
&= r_{o,s}^2(\mu) + R_n(0; m). \quad \text{(A-1)}
\end{aligned}
$$

Thus

$$
\begin{aligned}
E\{e_m\} &= \int\limits_{(m-X_c)T_{\text{ps}}-\frac{\epsilon\tau}{2}}^{(m-X_c)T_{\text{ps}}+\frac{\epsilon\tau}{2}} E\left\{|r_{\text{out}}(\mu)|^2\right\} d\mu \\
&= \int\limits_{(m-X_c)T_{\text{ps}}-\frac{\epsilon\tau}{2}}^{(m-X_c)T_{\text{ps}}+\frac{\epsilon\tau}{2}} \left(r_{o,s}^2(\mu) + R_n(0; m)\right) d\mu \\
&\cong \nu_m G E_0 \rho_\epsilon \delta_K(m-d) + \epsilon\tau R_n(0; m) \quad \text{(A-2)}
\end{aligned}
$$

where the last approximation follows from (11).

The autocorrelation function is given by

$$
\begin{aligned}
E\left\{|r_{\text{out}}(\mu_1)|^2|r_{\text{out}}(\mu_2)|^2\right\} &= E\left\{|r_{o,s}(\mu_1) + r_{o,n}(\mu_1)|^2 \right.\\
&\quad \left. \times |r_{o,s}(\mu_2) + r_{o,n}(\mu_2)|^2\right\} \\
&= r_{o,s}^2(\mu_1)r_{o,s}^2(\mu_2) + r_{o,s}^2(\mu_1) \\
&\quad \times R_n(0; m) + r_{o,s}^2(\mu_2) \\
&\quad \times R_n(0; m) + 2r_{o,s}(\mu_1) \\
&\quad \times r_{o,s}(\mu_2)R_n(\mu_1 - \mu_2; m) \\
&\quad + E\left\{|r_{o,n}(\mu_1)|^2\right. \\
&\quad \left. \times |r_{o,n}(\mu_2)|^2\right\} \quad \text{(A-3)}
\end{aligned}
$$

where the last equality follows from the facts that the expectation of odd-order terms of $r_{o,n}(\mu)$ is zero and that $E\{r_{o,n}(\mu_1)r_{o,n}(\mu_2)\} = 0$. On the other hand, we have

$$
\begin{aligned}
E\left\{|r_{o,n}(\mu_1)|^2|r_{o,n}(\mu_2)|^2\right\} &= E\left\{\left(n_r^2(\mu_1) + n_i^2(\mu_1)\right)\right.\\
&\quad \left. \times \left(n_r^2(\mu_2) + n_i^2(\mu_2)\right)\right\} \\
&= \frac{1}{2}R_n^2(0; m) \\
&\quad + E\left\{n_r^2(\mu_1)n_r^2(\mu_2)\right\} \\
&\quad + E\left\{n_i^2(\mu_1)n_i^2(\mu_2)\right\}. \quad \text{(A-4)}
\end{aligned}
$$

Let us denote $\sigma^2 = E\{n_r^2(\mu)\} = E\{n_i^2(\mu)\} = 1/2R_n(0; m)$ and $\rho = (R_n(\mu_1 - \mu_2; m))/(R_n(0; m))$. Then, we get

$$
\begin{aligned}
E\left\{n_r^2(\mu_1)n_r^2(\mu_2)\right\} &= \frac{1}{2\pi\sigma^2\sqrt{1-\rho^2}} \int\limits_{-\infty}^{\infty}\int\limits_{-\infty}^{\infty} x^2 y^2 \\
&\quad \times \exp\left(-\frac{x^2 - 2\rho xy + y^2}{2\sigma^2(1-\rho^2)}\right) dx\,dy \\
&= (1+2\rho^2)\sigma^4 \\
&= \frac{1}{4}R_n^2(0; m) + \frac{1}{2}R_n^2(\mu_1 - \mu_2; m). \quad \text{(A-5)}
\end{aligned}
$$

Since $E\{n_i^2(\mu_1)n_i^2(\mu_2)\}$ yields the same result, we have $E\{|r_{o,n}(\mu_1)|^2|r_{o,n}(\mu_2)|^2\} = R_n^2(0; m) + R_n^2(\mu_1 - \mu_2; m)$.

Therefore, we have

$$
\begin{aligned}
\mathrm{Var}\{e_m\} &= \int_{(m-X_c)T_{\mathrm{ps}}-\frac{\epsilon\tau}{2}}^{(m-X_c)T_{\mathrm{ps}}+\frac{\epsilon\tau}{2}} \int_{(m-X_c)T_{\mathrm{ps}}-\frac{\epsilon\tau}{2}}^{(m-X_c)T_{\mathrm{ps}}+\frac{\epsilon\tau}{2}} \\
&\quad \times \left(E\left\{|r_{\mathrm{out}}(\mu_1)|^2 \cdot |r_{\mathrm{out}}(\mu_2)|^2\right\} \right.\\
&\quad \left. - E\left\{|r_{\mathrm{out}}(\mu_1)|^2\right\} E\left\{|r_{\mathrm{out}}(\mu_2)|^2\right\} \right) d\mu_1 d\mu_2 \\
&= \int_{(m-X_c)T_{\mathrm{ps}}-\frac{\epsilon\tau}{2}}^{(m-X_c)T_{\mathrm{ps}}+\frac{\epsilon\tau}{2}} \int_{(m-X_c)T_{\mathrm{ps}}-\frac{\epsilon\tau}{2}}^{(m-X_c)T_{\mathrm{ps}}+\frac{\epsilon\tau}{2}} \\
&\quad \times \left(2r_{o,s}(\mu_1)r_{o,s}(\mu_2)\cdot R_n(\mu_1-\mu_2;m) \right.\\
&\quad \left. + R_n^2(\mu_1-\mu_2;m) \right) d\mu_1 d\mu_2 \\
&\cong \int_{-\frac{\epsilon\tau}{2}}^{\frac{\epsilon\tau}{2}} \int_{-\frac{\epsilon\tau}{2}}^{\frac{\epsilon\tau}{2}} \left(2r_{o,s}(\mu_1)r_{o,s}(\mu_2)R_n(\mu_1-\mu_2;m) \right.\\
&\quad \left. \times \delta_K\,(m-d) + R_n^2(\mu_1-\mu_2;m) \right) d\mu_1 d\mu_2
\end{aligned}
$$

(A-6)

where the last approximation also follows from (11).

APPENDIX B

EVALUATION OF THE UNION BOUND ON THE BIT-ERROR PROBABILITY IN THE MPT SCHEME

Since we have β OOCs and J users, an OOC is assigned to $C = \lceil J/\beta \rceil$ users in a group, where $\lceil a \rceil$ denotes the smallest integer greater than a. Then, an interferer from other groups can corrupt one pulse of the desired user with probability $(w^2)/(F)$ [19]. On the other hand, an interferer from the same group can corrupt one pulse and all w pulses of the desired user with probability $(w^2 - w)/(F)$ and $1/F$, respectively. Let a_1, a_2, and a_3 be the numbers of w-pulse corrupting interferers from the same group, one-pulse corrupting interferers from the same group, and one-pulse corrupting interferers from another group, respectively. Then, the probability of this event is

$$
\begin{aligned}
\mathrm{Pr}\{a_1, a_2, a_3\} &= \binom{C}{a_1}\left(\frac{1}{F}\right)^{a_1}\binom{C-a_1}{a_2}\left(\frac{w^2-w}{F}\right)^{a_2} \\
&\quad \cdot \binom{J-1-C}{a_3}\left(\frac{w^2}{F}\right)^{a_3} \\
&\quad \cdot \left(1-\frac{w^2}{F}\right)^{J-1-a}
\end{aligned}
$$

(B-1)

where $a = a_1 + a_2 + a_3$. For given values of a_1, a_2, and a_3, we generate λ_j with uniform distribution over $[-T_{\mathrm{sl}}/2, T_{\mathrm{sl}}/2]$. We also select $\iota_j \in \{1, \cdots, w\}$ equiprobably to locate the jth interferer around the ι_jth pulse location of the desired user. We then evaluate $l_{d,i} = \sum_{j=1}^{a_1}\mathrm{sinc}^2(\Omega\lambda_j) + \sum_{j=a_1+1}^{a}\delta_K(i-\iota_j)\mathrm{sinc}^2(\Omega\lambda_j)$ and $l_{r,i} = \sum_{j=1}^{a_1}\mathrm{sinc}^2(\Omega(rT_{\mathrm{ps}}-\lambda_j)) + \sum_{j=a_1+1}^{a}\delta_K(i-\iota_j)\mathrm{sinc}^2(\Omega(rT_{\mathrm{ps}}-\lambda_j))$. Here, we ignore sidelobes of the sinc^2 function, as we did in [1]. Then, we evaluate (31) and average it over $10\,000$ trials to obtain

$\mathrm{Pr}\{I_d < I_r|a_1, a_2, a_3\}$. Note that $\mathrm{Pr}\{I_d < I_r|0,0,0\} = 0$. Finally, the unconditional PEP and the union bound of the bit-error probability are obtained as

$$
\mathrm{Pr}\{I_d < I_r\} = \sum_{a_1=0}^{C}\sum_{a_2=0}^{C-a_1}\sum_{a_3=0}^{J-1-C} \mathrm{Pr}\{I_d < I_r|a_1, a_2, a_3\} \cdot \mathrm{Pr}\{a_1, a_2, a_3\}
$$

(B-2)

and

$$
P_b \leq \sum_{r=1}^{M-1}\frac{2(M-r)}{M}b(r)\,\mathrm{Pr}\{I_d < I_r\}
$$

(B-3)

respectively, where $b(r)$ is the average number of bit errors per number of bits in a symbol, caused by falsely detecting a symbol that is rT_{ps} apart from the desired symbol.

APPENDIX C

EVALUATION OF THE UNION BOUND ON THE SYMBOL-ERROR PROBABILITY IN THE ST SCHEME

The conditional PEP is given by [1]

$$
\mathrm{Pr}\{I_d < I_o|l_d, l_o\} = \frac{l_o}{l_d+l_o}\exp\left(-\frac{N_{\mathrm{eff}}}{l_d+l_o}\right), \quad l_d + l_o > 0
$$

(C-1)

where d and o are the transmitted and some other signal locations, respectively, and l_d and l_o are the effective numbers of interferers at the two signal locations, defined in [1]. Here, the subscript o is used to emphasize that the other signal location is in a different cluster. When the two signal locations are in the same cluster separated by rT_{ps} (subscript r is used instead of o in this case), the PEP is evaluated as in [1]. When the two signals are in different clusters with $\Omega T_{\mathrm{si}} \gg 1$, we can assume that an interferer that affects one signal location cannot affect the other signal location. Then, a modified version of the numerical method in [1] is applied to evaluate the PEP as follows. First, we assume that only interferers with time delays within $\pm T = \pm 1/\Omega$ of the two signal locations d and o are taken into account for l_d and l_o, respectively. Let a_1 and a_2 be the number of interferers with relative time delays within $\pm T$ of d and o. Then, we have

$$
\begin{aligned}
\mathrm{Pr}\{a_1, a_2\} &= \binom{J-1}{a_1}\binom{J-1-a_1}{a_2}\left(\frac{2T}{T_s}\right)^{a_1+a_2} \\
&\quad \cdot \left(1-\frac{2T}{T_s}\right)^{J-1-a_1-a_2}.
\end{aligned}
$$

(C-2)

For given values of a_1 and a_2, we generate λ_j with a uniform distribution over $[-T, T]$. Next, we evaluate $l_d = \sum_{j=1}^{a_1}\mathrm{sinc}^2(\Omega\lambda_j)$ and $l_o = \sum_{j=a_1+1}^{a_1+a_2}\mathrm{sinc}(\Omega\lambda_j)$. Then, we evaluate (C-1) and average it over $10\,000$ trials to obtain $\mathrm{Pr}\{I_d < I_o|a_1, a_2\}$. Again, note that $\mathrm{Pr}\{I_d < I_o|0,0\} = 0$. Finally, the unconditional PEP is obtained as

$$
\mathrm{Pr}\{I_d < I_o\} = \sum_{a_1=0}^{J-1}\sum_{a_2=0}^{J-1-a_1}\mathrm{Pr}\{I_d < I_o|a_1, a_2\}\mathrm{Pr}\{a_1, a_2\}.
$$

(C-3)

Since the PEP is the same for all $M(w-1)$ signal locations that are not in the same cluster of d, the symbol-error probability, P_s, is given by

$$P_s \leq \sum_{r=1}^{M-1} \frac{2(M-r)}{M} \Pr\{I_d < I_r\} + M(w-1)\Pr\{I_d < I_o\}$$

(C-4)

where the first term is the sum of PEP due to the signal locations in the same cluster, given in [1].

REFERENCES

[1] K. S. Kim, D. M. Marom, L. B. Milstein, and Y. Fainman, "Hybrid pulse position modulation/ultrashort light pulse code-division multiple-access systems—Part I: Fundamental analysis," *IEEE Trans. Commun*, vol. 50, pp. 2018–2031, Dec. 2002.

[2] P. C. Sun, Y. T. Mazurenko, and Y. Fainman, "Femtoscale pulse imaging: ultrafast optical oscilloscope," *J. Opt. Soc. Amer. A*, vol. 14, pp. 1159–1170, May 1997.

[3] D. M. Marom, D. Panasenko, P. C. Sun, and Y. Fainman, "Linear and nonlinear operation of a time-to-space processor," *J. Opt. Soc. Amer. A.*, vol. 18, pp. 448–458, Feb. 2001.

[4] J. W. Goodman, *Introduction to Fourier Optics*. New York: McGraw-Hill, 1968.

[5] E. Desurvire, *Erbium Doped Fiber Amplifiers, Principles and Applications*. New York: Wiley, 1994.

[6] S. Shen, C.-C. Chang, H. P. Sardesai, V. Binjrajka, and A. M. Weiner, "Effects of self-phase modulation on sub-500 fs pulse transmission over dispersion compensated fiber links," *J. Lightwave Technol.*, vol. 17, pp. 452–461, Mar. 1999.

[7] G. P. Agrawal, *Fiber-Optic Communication Systems*. New York: Wiley, 1993.

[8] H. J. Landau and H. O. Pollak, "Prolate spheroidal wave functions, Fourier analysis and uncertainty—III: the dimension of the space of essentially time- and band-limited signals," *Bell Syst. Tech. J.*, vol. 41, pp. 1295–1336, July 1962.

[9] P. A. Humblet and M. Azizoglu, "On the bit-error rate of lightwave systems with optical amplifiers," *J. Lightwave Technol.*, vol. 9, pp. 1576–1582, Nov. 1991.

[10] J.-S. Lee and C.-S. Shim, "Bit-error rate analysis of optically preamplified receivers using an eigenfunction expansion method in optical frequency domain," *J. Lightwave Technol.*, vol. 12, pp. 1224–1229, July 1994.

[11] S. Herbst, M. Baussman, and M. Erbacsh, "Sensitivity of a direct WDM-system with a frequency-selective optical receiver and optical preamplifier," *J. Lightwave Technol.*, vol. 12, pp. 32–36, Jan. 1998.

[12] M. Nakazawa, E. Yoshida, T. Yamamoto, E. Yamada, and A. Sahara, "TDM single channel 640 Gbit/s transmission experiment over 60 km using 400 fs pulse train and walk-off free, dispersion flattened nonlinear optical loop minor," *Electron. Lett.*, vol. 34, pp. 907–908, Apr. 1998.

[13] C.-C. Chang and A. M. Weiner, "Fiber transmission for sub-500-fs pulses using a dispersion-compensating fiber," *IEEE J. Quantum Electron.*, vol. 33, pp. 1455–1464, Sept. 1997.

[14] Y. Ding, A. M. Weiner, M. R. Melloch, and D. D. Nolte, "Adaptive all-order dispersion compensation of ultrafast laser pulses using dynamic spectral holography," *Appl. Phys. Lett.*, vol. 75, pp. 3255–3257, Nov. 1999.

[15] P. C. Sun, Y. T. Mazurenko, and Y. Fainman, "Real-time one-dimensional coherent imaging through single-mode fibers by space–time conversion processors," *Opt. Lett.*, vol. 22, pp. 1861–1863, Dec. 1997.

[16] G. Lenz, K. Tamura, H. A. Haus, and E. P. Ippen, "All-solid-state femtosecond source at 1.55 mu m," *Opt. Lett.*, vol. 20, pp. 1289–1291, June 1995.

[17] E. Yoshida and M. Nakazawa, "Ultrashort pulse generation at high repetition rate from mode-locked fiber lasers," *Rev. Laser Eng.*, vol. 27, pp. 274–280, Nov. 1999.

[18] T. Kurokawa, H. Tsuda, K. Okamoto, K. Naganuma, H. Takenouchi, Y. Inoue, and M. Ishii, "Time–space-conversion optical signal processing using arrayed-waveguide grating," *Electron. Lett.*, vol. 33, pp. 1890–1891, Oct. 1997.

[19] J. A. Salehi, "Code-division multiple-access techniques in optical fiber network—Part I: Fundamental principles," *IEEE Trans. Commun.*, vol. 37, pp. 824–833, Aug. 1989.

[20] J. G. Proakis, *Digital Communication*, 3rd ed. New York: McGraw-Hill, 1995.

[21] A. H. S. Mohammadi and A. K. Khandani, "Unequal error protection on turbo-encoder output bits," *Electron. Lett.*, vol. 33, pp. 273–274, Feb. 1997.

Kwang Soon Kim (S'94–M'99) was born in Seoul, Korea, on September 20, 1972. He received the B.S. (*summa cum laude*), M.S.E., and Ph.D. degrees in electrical engineering from the Korea Advanced Institute of Science and Technology (KAIST), Daejeon, Korea, in 1994, 1996, and 1999, respectively.

He was a Teaching and Research Assistant at the Department of Electrical Engineering, KAIST, from March 1994 to February 1999. From March 1999 to March 2000, he was with the Department of Electrical and Computer Engineering, University of California at San Diego, La Jolla, as a Postdoctoral Researcher. In April 2000, he joined the Mobile Telecommunication Research Laboratory, Electronics and Telecommunication Research Institute, Daejeon, Korea, where he is currently a Senior Member of Research Staff. His research interests include detection and estimation theory, channel coding and iterative decoding, array signal processing, wireless/optical CDMA systems, wireless CDMA MODEM design and development, and wireless OFDM systems.

Dr. Kim received the Postdoctoral Fellowship from the Korea Science and Engineering Foundation (KOSEF) in 1999. He also received the Silver Prize at the Humantech Paper Contest in 1998, the Silver Prize at the LG Information and Communications Paper Contest in 1998, and the Best Researcher Award from the Electronics and Telecommunication Research Institute (ETRI) in 2002.

Dan M. Marom (S'98–M'01) was born in Detroit, MI, in 1967. He received the B.Sc. and M.Sc. degrees from Tel-Aviv University, Tel-Aviv, Israel, in 1989 and 1995, respectively, and the Ph.D. degree from the University of California, San Diego (UCSD), in 2000. His doctoral dissertation dealt with femtosecond-rate optical signal processing with applications in ultrafast communications.

From 1996 through 2000, he was a Fannie and John Hertz Foundation Graduate Fellow at UCSD. In 2000, he joined Bell Laboratories, Holmdel, NJ, to pursue his interests in optical communications.

Dr. Marom received the IEEE Lasers and Electro-Optics Society Best Student Paper Award in 1999.

Laurence B. Milstein (S'66–M'68–SM'77–F'85) received the B.E.E. degree from the City College of New York, New York, NY, in 1964, and the M.S. and Ph.D. degrees in electrical engineering from the Polytechnic Institute of Brooklyn, Brooklyn, NY, in 1966 and 1968, respectively.

From 1968 to 1974, he was with the Space and Communications Group of Hughes Aircraft Company, and from 1974 to 1976, he was a member of the Department of Electrical and Systems Engineering, Rensselaer Polytechnic Institute, Troy, NY. Since 1976, he has been with the Department of Electrical and Computer Engineering, University of California at San Diego, La Jolla, where he is a Professor and former Department Chairman, working in the area of digital communication theory with special emphasis on spread-spectrum communication systems. He has also been a consultant to both government and industry in the areas of radar and communications.

Dr. Milstein was an Associate Editor for Communication Theory for the IEEE TRANSACTIONS ON COMMUNICATIONS, an Associate Editor for Book Reviews for the IEEE TRANSACTIONS ON INFORMATION THEORY, an Associate Technical Editor for the *IEEE Communications Magazine*, and the Editor-in-Chief of the IEEE JOURNAL ON SELECTED AREAS IN COMMUNICATIONS. He was the Vice President for Technical Affairs in 1990 and 1991 of the IEEE Communications Society, and has been a member of the Board of Governors of both the IEEE Communications Society and the IEEE Information Theory Society. He is a former Chair of the IEEE Fellows Selection Committee, and a former Chair of ComSoc's Strategic Planning Committee. He is a recipient of the 1998 Military Communications Conference Long Term Technical Achievement Award, an Academic Senate 1999 UCSD Distinguished Teaching Award, an IEEE Third Millenium Medal in 2000, the 2000 IEEE Communication Society Armstrong Technical Achievement Award, and the 2002 MILCOM Fred Ellersick Award.

Yeshaiahu Fainman (M'93–SM'01–F'03) received the Ph.D. degree from Technion-Israel Institute of Technology, Haifa, Israel, in 1983.

He is a Professor of Electrical and Computer Engineering at the University of California at San Diego, La Jolla. His current research interests are in nonlinear space–time processes using femtosecond laser pulses for optical communications, near-field phenomena in optical nanostructures and nanophotonic devices, quantum cryptography and communication, 3-D quantitative imaging, programmable, multifunctional diffractive, and nonlinear optics. He contributed over 100 manuscripts in referred journals and over 170 conference presentations and conference proceedings. Between 1993–2001, he served as a Topical Editor of the *Journal of the Optical Society of America: A* on Optical Signal Processing and Imaging Science.

Dr. Fainman is a Fellow of the Optical Society of America and a recipient of the Miriam and Aharon Gutvirt Prize. He served on several conferences' program committees, and organized symposia and workshops.